www.ietdl.org

Published in IET Microwaves, Antennas & Propagation
Received on 13th January 2011
Revised on 6th May 2011
doi: 10.1049/iet-map.2011.0029

ISSN 1751-8725

Radiofrequency MEMS-enabled polarisation-reconfigurable antenna arrays on multilayer liquid crystal polymer

G. Wang[1] *R. Bairavasubramanian*[2] *B. Pan*[3] *J. Papapolymerou*[4]

[1]*Department of Electrial Engineering, The University of South Carolina, Columbia, SC, USA*
[2]*Skyworks Solutions Inc., Boise, ID, USA*
[3]*Broadcom Corporation, Irvine, CA, USA*
[4]*School of Electrical and Computer Engineering, Georgia Institute of Technology, Atlanta, GA 30332, USA*
E-mail: gwang@engr.sc.edu

Abstract: The development of polarisation-reconfigurable antenna arrays on multilayer liquid crystal polymer (LCP) technology for remote sensing applications is presented for the first time. Two 2 × 2 antenna arrays operating at 14 and 35 GHz have been designed, fabricated and measured. These arrays use printed patch antenna elements and can operate in two linear orthogonal polarisations, one at a time. Switching between the polarisations is achieved using microelectromechanical systems (MEMS) that are integrated with the arrays. It is well known that the performance of patch antennas depends strongly on the characteristics of the substrate. In addition, the application under consideration (remote sensing) puts stringent requirements on the underlying material technology. Specifically, the material technology needs to support large area processing, multilayer implementation and easy deployment in space. LCP, with a unique combination of characteristics and good millimeter wave performance, offers an excellent solution. Its flexible properties allow for the material to be rolled up and deployed in space. The array design methodology together with fabrication of radiofrequency MEMS switches on LCP is discussed. Scattering parameter and radiation pattern measurements are included.

1 Introduction

Many radar and communication systems require antennas equipped with dual-polarisation capabilities that give a higher capacity of data transfer. Dual-polarised antennas have been used to increase the number of subchannels [1] in multiple-input multiple-output mobile communications systems. In automotive radar systems, dual-polarised antennas can also be used to detect potential road hazards [2], such as black ice, that have a cross section with one dimension being much thinner than the perpendicular direction. Moreover, dual-frequency antennas have gained interest in wireless communication systems where different frequency applications, including wireless local area networks (WLANs-802.11a, b, g) and personal communication services can be covered in a single design. Over the last 30 years, antenna arrays have been utilised in various applications owing to their directive main beam and high gain characteristics for long-range communication. Microstrip patch antennas are often desirable antenna elements owing to their low cost, low profile, light weight and ease of fabrication characteristics [3].

To achieve dual-polarisation or/and dual-frequency reconfigurable antenna array, either a 'dual-feed' technique [4] or serial corner feeding [5] has been introduced. Those methods require multi-feed and complex matching networks to achieve high isolation between the input ports. A pin diode controlled switching technique for reconfigurable dual-frequency operation has recently been reported [6, 7] to obtain compact design of antenna minimising the feed and matching network. With the superb radiofrequency (RF) performance of RF MEMS switch, reconfigurable RF MEMS antenna systems were first introduced in 1998 by Brown [8] and since then have been studied by several research groups. An emphasis has been given in reconfigurable aperture (recap) and microstrip antenna structures, to achieve multiple octave tunability [9–12]. Still, the integration of RF MEMS with the antenna has not been fully demonstrated [13, 14], especially RF MEMS switch tuning of microstrip patch antenna arrays having dual-frequency and dual-polarisation operation is not much explored.

In addition, to integrate switches and phase shifters to the antenna array, thus taking full advantage of polarisation diversity and beam scanning capabilities, there is a need for a laminated substrate that is suitable for packaging RF passive and active components and embedded functions. Although there have been many reported examples of dual frequency, dual polarisation microstrip antenna arrays on substrates, such as Duroid, these designs are not always favourable for a radio frequency (RF) system-on-a-package (SOP) low-cost technology owing to various undesirable substrate properties. Liquid crystal polymer (LCP) has

gained much consideration as a potential high-performance microwave substrate and packaging material. Its low dielectric constant ($\varepsilon_r = 3.0$) and low loss performance ($\tan\delta = 0.002 - 0.004$ for frequency less than 35 GHz) is a key feature in minimising dielectric and surface wave losses. Moreover, the near hermetic nature of the materials (water absorption less than 0.04%), the flexibility and the relatively low processing temperatures enable the design of conformal antenna arrays, the integration of RF MEMS devices, and the low deployment costs in space applications from rolling antennas on LCP. The low water absorption of LCP makes the material stable in a variety of environmental conditions, hence, preventing changes in the materials' dielectric constant and loss tangent. The multilayer circuitry can be easily realised owing to the two types of LCP substrates that have different melting temperatures: the high melting temperature LCP (around 315°C) is primarily used as the core substrate layer, whereas the low melting temperature LCP (around 290°C) is used as a bonding layer. Therefore vertical integration can be achieved similarly to low temperature co-fired ceramic (LTCC).

A single pole single through RF MEMS switch on LCP substrate was first reported in [15]. It demonstrated the possibility of integration of single RF MEMS switch on flexible polymer substrate. The fabrication of RF MEMS switch on LCP substrate is discussed in [15]. The organisation of this paper is as follows: A summary of RF MEMS switch on LCP is presented in Section 2 followed by the description of antenna array design, fabrication and measurement results of the integrated array in Section 3 and a brief conclusion. The design presented here can eventually be applied to the remote sensing of precipitation at 14 and 35 GHz. The measured S parameters and radiation pattern of the antenna array are shown in the paper.

2 RF MEMS switch on LCP

High C_{ON}/C_{OFF} ratio is very critical for RF MEMS capacitive switches. In order to obtain high capacitance when the switch is at the down state, good contact between the switch membrane and bottom signal line is needed. However, the surface roughness of bare LCP normally is around 0.6–1 μm, and thus, decreases the performance of the switch at the ON state (the membrane is on the down position). Two different methods have been used to smooth the surface roughness of LCP [15, 16]. In the first method, a 3 μm PI2610 polyimide is first spun on LCP to planarise the surface to minimise the roughness. This results to a measured surface roughness of around 500 Å. In the second method, LCP was polished using Lap Master Polisher with 0.06 μm slurry for 2 h and the surface roughness was measured around 600 Å (0.06 μm). To fabricate MEMS switches on the LCP substrate, a simple four mask process was used. A little bit thicker bottom metal layer was patterned to improve the surface roughness of the substrate.

Measurements of the air-bridge type switch were taken using an Agilent 8510 network analyser. A thru-line-reflect (TRL) calibration was also performed to de-embed the co-planar line and transition. Measured results for the nitride switches with LCP coated with polyimide and polished LCP are shown in Fig. 1 and summarised in Table 1. A silicon nitride layer was deposited by plasma enhanced chemical vapour deposition (PECVD) for 30 min for all the switches. Different C_{ON} are achieved between the switches with different substrates, this is caused by the slightly different deposition rate of silicon nitride on different

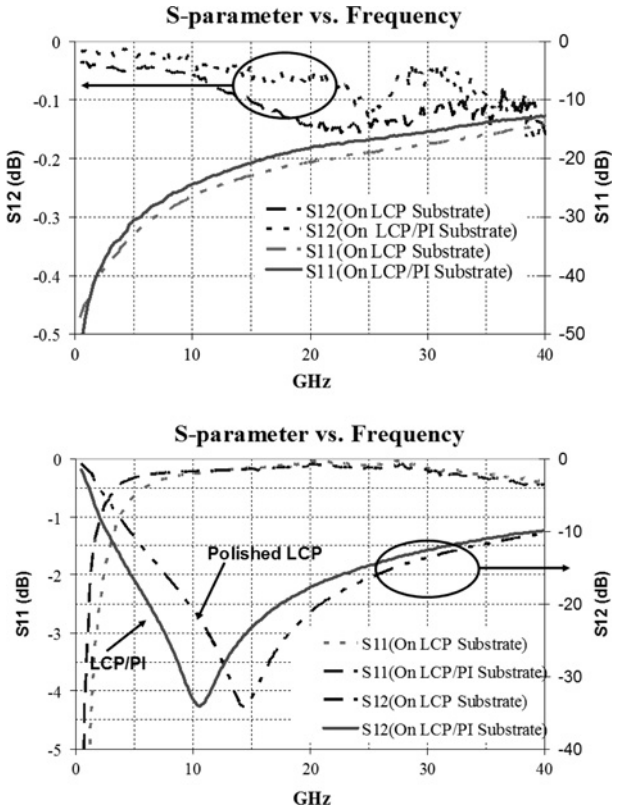

Fig. 1 *Measured S-parameters of the fabricated airbridge type switch on up state (top) and down state (bottom)*

Table 1 Measured *S*-parameter summary for airbridge type switch on different substrates

Substrate	Up state insertion loss, dB	Up state return loss, dB	Down state isolation loss, dB	Down state return loss, dB
LCP/PI	0.08	18	17.7	0.1
LCP	0.05	20.6	20.8	0.05

substrates. The thickness of deposited silicon nitride on LCP with polymide layer and polished LCP are 2600 and 3000 Å, respectively. All airbridge switches with LCP substrate have very low insertion loss; this is probably partly due to the low dielectric loss tangent of the LCP substrate, The insertion loss for the on-state and return loss for the off-state for switch on polymide coated LCP substarte is slightly higher than that of switches on LCP substrate, this is partly due to the higher loss of polyimide layer. Also, to obtain stable and accurate measurement results, it is very important to obtain good measurement contacts since the LCP substrate is flexible.

3 Aperture-coupled patch antenna arrays

The generic multilayer architecture of the developed aperture-coupled array is shown in Fig. 2.

The total substrate thickness is approximately 460 μm. The radiating elements for both arrays are placed on one side of the ground plane, while the feed network for both arrays is placed on the other side. The ground plane contains slots through which energy is electromagnetically coupled from the feed network to the radiating patches. With the ground

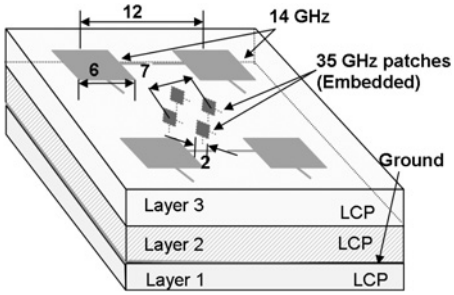

Fig. 2 *Generic multilayer architecture of the aperture-coupled antenna array*

plane taken as the reference, the 35 GHz patches are placed on a 125 μm thick LCP substrate, whereas the 14 GHz patches are placed on a 355 μm thick LCP substrate. The feed networks for both patches are placed on a 100 μm thick LCP substrate on the other side of the ground plane. Although many possibilities of substrate and feed configurations exist, this arrangement was particularly chosen to meet three major requirements of this application

1. The return loss and radiation characteristics for both polarisations need to be identical.
2. The return loss and radiation characteristics for both frequencies need to be similar.
3. Polarisation reconfigurabilty and beam steering requires integration of antenna arrays with electronic or electromechanical switches, phase shifters and attenuators.

The top view of the designed aperture-coupled array, showing the switch locations and bias pads, is depicted in Fig. 3.

As shown in Fig. 3, a combination of series and parallel feed was employed to form the 2×2 array. Each 2×2 array consists of two linear 2×1 arrays. The most popularly used feed network for the formation of large arrays is the corporate feed network. In a corporate feed, all radiating elements are interconnected in a parallel feed configuration, so that uniform amplitude and phase distribution can be easily achieved. On the other hand, a series feed can result in a reduction of the overall length of the feed network and hence can reduce the associated feedline losses. The disadvantages of the series feed are beam-drifting and difficulties in achieving the desired amplitude distribution across the array. To take advantage

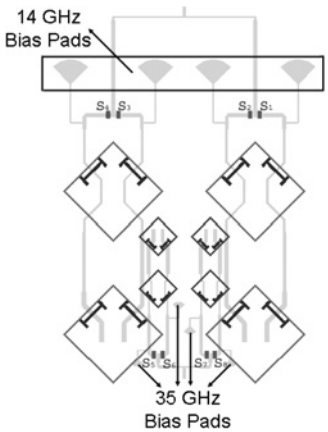

Fig. 3 *Polarisation-reconfigurable aperture-showing switch locations and bias pads*

of the characteristic features of both types of feed network, a combination of series and parallel feeds was used in this design. In the past, series feed networks have been employed with resistor terminations. Although this is an effective method to design a series feed, it reduces the overall efficiency. In our work, we used a radiating element itself as a terminating element, thereby improving the overall efficiency of the array.

The advantages of the developed aperture-coupled arrays include

- No or minimum parasitic radiation from feed lines. This is expected to reduce distortion in the radiation pattern.
- For polarisation reconfigurability, all switches can be placed in the same layer. This may significantly reduce the overall fabrication cost and complexity.
- For an $N \times M$ array, the number of switches required is only $2N$. This is because of the use of series feed along one dimension of the array.

The location and the orientation of the bias pads and radial stubs are slightly modified for the 35 GHz array to efficiently utilise the available space. This configuration also minimises the interaction between various stubs and the feed network. The total length of each radial stub is adjusted to produce an open at the operating frequency. The transformers and the combiners of the corporate feed network were optimised to minimise the effects of the bias stubs on the resonant frequency of the arrays. The polarisation of both 14 and 35 GHz arrays is controlled by the configuration of the MEMS switches. As dedicated feed network and MEMS switches are provided for the two antenna arrays, the polarisation of one array can be chosen independent of the other.

Table 2 shows the different configuration of switches that can be used to enforce the desired linear polarisation for a particular array.

Other switch configurations are also possible. The listed configurations are the most useful for the proposed application. Measurements were not made for the last two states outlined in the table ($a5$ and $a6$), because of setup constraints. These two states require simultaneous excitation of the array at two frequencies.

3.1 Fabrication of antenna array

The antenna arrays were fabricated with double copper-clad LCP dielectric sheets from Rogers Corporation. The 14 GHz antenna array was fabricated on a 9 mm thick LCP substrate, whereas the 35 GHz antenna array was fabricated on a 5 mm thick LCP substrate, and a slotted ground was fabricated on the top side of a 4 mm LCP substrate. A standard photolithographic process was used for all the fabrication. The three LCP layers were bonded together following the sequence as shown in Fig. 2 with thermal compressive bonding technique using Karl Suss Bonder. Before the fabrication of the feeding network, the bottom side of the bonded LCP layers were polished to improve the surface smoothness. A Ti/Au layer was then evaporated and patterned on the polished side of the LCP layer to form the feeding network; the alignment was done through the laser etched alignment holes on the LCP. A 2000 Å silicon nitride was then deposited using plasma enhanced chemical vapour deposition at 150°C to avoid the melting of the LCP layer. The nitride layer was then patterned and etched with RIE, a 3 μm thick photoresist was then spin coated and patterned to form the airgap for the MEMS switch. After

doi: 10.1049/iet-map.2011.0029

Table 2 Switch configurations for the polarisation-reconfigurable antenna array

State	Switches that are 'ON'	Switches that are 'OFF'	14 GHz	35 GHz
*a*0	none	all	not excited	not excited
*a*1	*S*1, *S*3	*S*2, *S*4, *S*5, *S*6, *S*7, *S*8	Pol-I	not excited
*a*2	*S*2, *S*4	*S*1, *S*3, *S*5, *S*6, *S*7, *S*8	Pol-II	not excited
*a*3	*S*5, *S*7	*S*1, *S*2, *S*3, *S*4, *S*6, *S*8	not excited	Pol-I
*a*4	*S*6, *S*8	*S*1, *S*2, *S*3, *S*4, *S*5, *S*7	not excited	Pol-II
*a*5	*S*1, *S*3, *S*5, *S*7	*S*2, *S*4, *S*6, *S*8	Pol-I	Pol-I
*a*6	*S*2, *S*4, *S*6, *S*8	*S*1, *S*3, *S*5, *S*7	Pol-II	Pol-II

that, Ti/Au/Ti seed layer was evaporated and electroplated to 3 μm thick. The final step is etching the seed layer and releasing the structure. During the whole fabrication, the other side of the sample was protected with a thick layer of photoresist. Fig. 4 shows a close-up view of the fabricated MEMS switches.

3.2 S parameters and radiation pattern measurements

Scattering parameter measurements were made for both the 14 and 35 GHz arrays. A co-planar waveguide-strip transition was used and a TRL calibration set-up was utilised to de-embed the effects of the transition. When the 14 GHz array was excited, the 35 GHz array was treated as a parasitic element and vice versa. DC probes were used to actuate the MEMS switches.

Figs. 5 and 6 show the scattering parameter performance of the arrays for different switch configurations. For the 14 GHz array, when polarisation-I is excited, the resonant frequency is 14.7 GHz and when polarisation-II is excited, the resonant frequency is 14.8 GHz. For the 35 GHz array, when polarisation-I is excited, the resonant frequency is 36.6 GHz and when polarisation-II is excited, the resonant frequency is 36.4 GHz. The resonant frequency shift between the polarisations most likely resulted from fabrication inaccuracies. The resonant frequency of a patch antenna is strongly coupled to the length of the antenna. A higher over-etch along one dimension along one dimension could have resulted in the observed frequency shift. A lot of manual fabrication is involved in creating these prototypes. A better process controlled fabrication might help minimise such errors. When all the switches are in the 'OFF' state,

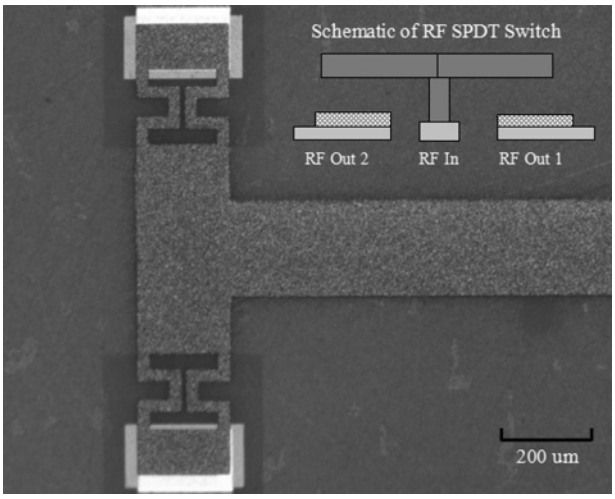

Fig. 4 *Close-up view of a fabricated MEMS switch*

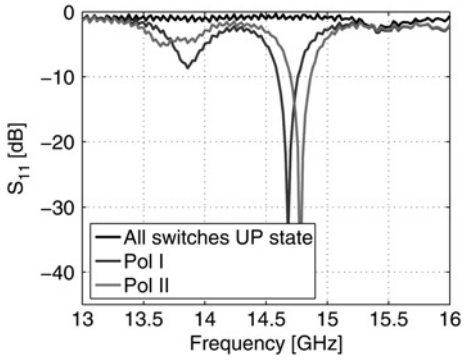

Fig. 5 *Return loss – 14 GHz aperture-coupled array with MEMS*

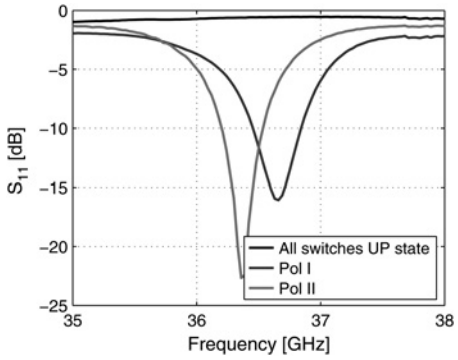

Fig. 6 *Return loss – 35 GHz aperture-coupled array with MEMS*

the radiating patches are not excited and the expected return loss level is 0 dB. This value is −0.8 dB for the 14 GHz array and −0.6 dB for the 35 GHz array. These figures represent the feed line losses and are satisfactory compared to the return loss levels when the patches are excited in one of the two polarisations. Apart from the losses, a negligible amount of energy might have coupled to the radiating patches because of the 'OFF' state capacitance of the MEMS switches.

The impedance characteristics are summarised in Tables 3 and 4. The measured bandwidth is about 1.1–1.2%, which has met the bandwidth requirement (1%) for the desired applications.

Radiation patterns are shown in Figs. 7 and 8 for the *E*- and *H*-plane at 14 GHz, respectively, and Figs. 9 and 10 for the *E*- and *H*-plane at 35 GHz, respectively. The antenna array is simulated with RF MEMS switch set as perfect open and short. The *E*- plane and *H*-plane beamwidths and the shapes of the co-polarised patterns are consistent for both the simulated and measured patterns of the arrays which is expected for a symmetric configuration. Radiation patterns

Table 3 Return loss characteristics of the 14 GHz aperture-coupled array

Characteristic	Pol-I	Pol-II
resonant frequency	14.7 GHz	14.8 GHz
return loss	−31 dB	−40 dB
−10 dB return loss bandwidth	180 MHz	180 MHz
percent bandwidth	1.2%	1.2%

Table 4 Return loss characteristics of the 35 GHz aperture-coupled array

Characteristic	Pol-I	Pol-II
resonant frequency	36.6 GHz	36.4 GHz
return loss	−16 dB	−22 dB
−10 dB return loss bandwidth	390 MHz	380 MHz
percent bandwidth	1.1%	1.1%

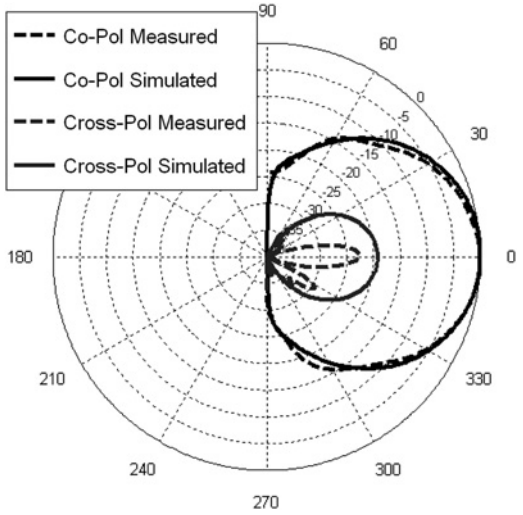

Fig. 7 *E-plane radiation pattern – 14 GHz*

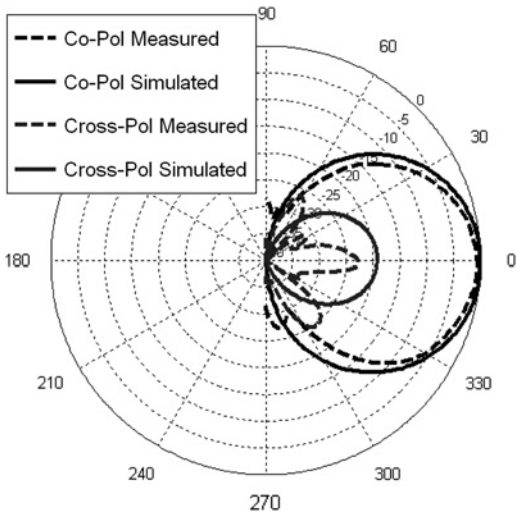

Fig. 8 *H-plane radiation pattern – 14 GHz*

were taken in an anechoic chamber equipped with the Nearfield Systems Inc. (NSI) near-field radiation patterning acquisition system. To facilitate radiation pattern measurement in such

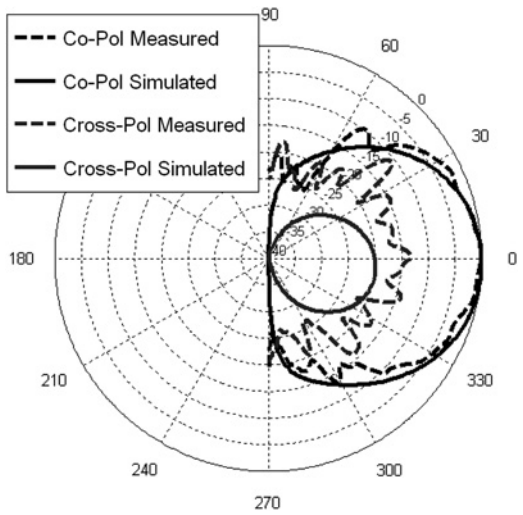

Fig. 9 *E-plane radiation pattern – 35 GHz*

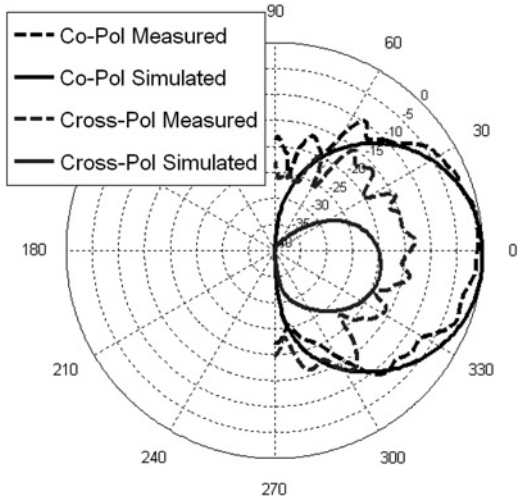

Fig. 10 *H-plane radiation pattern – 35 GHz*

environment at high frequency, perfect short and open condition was again used to emulate MEMS switch whose function was validated earlier. Bias lines were included to make sure their effects on the radiation pattern are included. As expected, since the use of slot feeding mechanism provides excellent isolation between the radiating elements and the feeding/biasing networks, no disturbance from the feeding/biasing networks has been observed in both simulation and measurement.

For each frequency (14 and 35 GHz), radiation patterns were measured on 45 and 135° planes (*E*- and *H*-plane) for both polarisation. Owing to the symmetric configuration of the whole array, measured patterns of each polarisation are identical to each other except for the polarisation swapping. The radiation pattern measurements did not show any significant beam drifting. Both arrays showed peak directivity at broadside. The prototype built was only a 2×2 array and achieving uniform amplitude and phase across the elements was not difficult. The problem could be more pronounced in a larger array. In addition, beam drifting against frequency may not be a significant issue for the application of concern as the bandwidth requirement is very minimal. As shown in Figs. 7–10, the measured patterns are consistent with the simulated results.

doi: 10.1049/iet-map.2011.0029

Table 5 Efficiency calculations of the 14 GHZ aperture-coupled array

measured efficiency (Wheeler Cap method)	58.6%
mismatch loss, dB	0.00 (100%)
connector loss, dB	0.15 (96.6%)
feedline loss, dB	1 (79.55)
total loss, dB	1.15 (76.7%)
de-embedded efficiency	76.4%

3.3 Efficiency calculations

Apart from the return loss and the radiation pattern measurements, efficiency measurements were also carried out. The efficiency of the 2×2 14 GHz aperture-coupled array was measured using the Wheeler Cap Method, with cap dimensions of 10.8 mm $\times$ 34 mm $\times$ 65 mm. The efficiency is calculated based on input resistance measurements. Two sets of resistance measurements were made – one with the cap and one without. When a cap with proper dimensions is used to enclose the sample, it is possible to reduce the radiation levels to a negligible amount so that the measured input resistance is a measure of various losses only. The measurement without the cap is a measure of the total input resistance (i.e. the radiation resistance and the loss resistance). From the two measurements, the radiation efficiency can be calculated. The radiation efficiency of the antenna is given by

$$\eta_{\text{rad}} = \frac{R_{\text{rad}}}{R_{\text{rad}} + R_{\text{loss}}} \quad (1)$$

where η_{rad} is the radiation efficiency, R_{rad} is the radiation resistance and R_{loss} is the loss resistance.

The measured efficiency of the entire setup that includes the array, the feed network and the connector was 58.6%. To determine the efficiency of the antenna array only, it is necessary to de-embed the mismatch loss, the loss of the feed lines and the connector. The return loss plot of the array shows that the mismatch loss is negligible. The input feed line has been extended to facilitate scattering parameter and radiation pattern measurements. The losses of the extended feed line and the corporate feed network were determined based on the attenuation measurements reported in [17]. The typical connector loss at 14 GHz is 0.15 dB. After de-embedding these losses, the efficiency of the antenna array is found to be 76.4%. Table 5 shows a summary of the measured efficiency, specific losses and the de-embedded efficiency.

It should be noted that the feed line loss used in calculating the de-embedded efficiency included only the loss of the extended input feed and the main corporate branch. As a result, the calculated efficiency is only a conservative estimate. Despite this, the result compares favourably to the reported efficiencies of similar antenna arrays realised on other substrate technologies.

All the results shown are for one polarisation, but they are the same for the other orthogonal polarisation also because of the symmetric arrangement of radiating elements and the feed network.

4 Conclusion

The development of antenna arrays with dual frequencies and dual polarisations has been presented in multilayer LCP technology. Two 2×2 arrays operating at 14 and 35 GHz, respectively, have been designed. Their impedance and radiation characteristics have been validated with measurements. These arrays can be integrated with 3D modules containing integrated circuits, filters and embedded passives to realise a complete SOP-based RF front end. The arrays exhibit a return loss of better than 15 dB in both frequency bands. The results shown here demonstrate that using integrated MEMS switch on multilayer LCP laminates is a feasible solution in practical applications. The key challenge of integrating MEMS switch on such substrate has been solved. Antenna arrays with RF MEMS switch controlled polarisations introduce the possibility of a low-power reconfigurable antenna array design.

5 Acknowledgment

This work was supported by NASA's Earth Science and Technology Office under contract NNG05GP93G.

6 References

1 Degen, C., Keusgen, W.: 'Performance evaluation of MIMO systems using dual-polarized antennas'. Tenth Int. Conf. on Telecommunications, ICT2003, March 2003, pp. 1520–1525
2 Mura, S., Gearhart, S.: 'Dual-polarized slotcoupled patch antennas on duroid with teflon lenses for 76.5-GHz automotive radar systems', *IEEE Trans. Antennas Propag.*, 1999, **47**, pp. 1836–1842
3 Garg, B.: 'Microstrip antenna design handbook' (Wiley, New York, NY, 2001)
4 Wong, H., Lau, K.-L., Luk, K.-M.: 'Design of dual-polarized l-probe patch antenna arrays with high isolation', *IEEE Trans. Antennas Propag.*, 2004, **52**, (1), pp. 45–52
5 Gao, S., Zhong, S.: 'A dual-polarized microstrip antenna array with high isolation fed by Coplanar network'. Proc. RAWCON'98, pp. 213–216
6 Shynu, S.V., Aanandan, C.K., Mohanan, P., Vasudevan, K.: 'A compact electronically reconfigurable dual frequency microstrip antenna for lband applications', *Int. J. Wirel. Opt. Commun.*, 2004, **2**, (2), pp. 181–187
7 Shynu, S.V., Augustin, G., Aanandan, C.K., Mohanan, P., Vasudevan, K.: 'Design of compact reconfigurable dual frequency micostrip antennas using varactor diodes', *Prog. Electromagn. Res., PIER*, 2006, **60**, pp. 197–205
8 Brown, E.R.: 'RF MEMS switches for reconfigurable integrated circuits', *IEEE Trans. Microw. Theory Tech.*, 1998, **46**, pp. 1868–1880
9 Chiao, J.C., Fu, Y., Chio, J.M., DeLisio, M., Lin, L.Y.: 'MEMS reconfigurable antenna'. IEEE MTT-S Int. Microwave Symp. Digest, June 1999, vol. 2, pp. 1515–1518
10 Weedon, W., Payne, W., Rebeiz, G., Herd, J., Champion, M.: 'MEMS switched reconfigurable multi-band antenna: design and modeling'. Proc. Antenna Applications Symp., June 1999, vol. 2, pp. 1525–1528
11 Brown, E.: 'On the gain of a reconfigurable aperture antenna', *IEEE Trans. Antenna Propag.*, 2001, **10**, pp. 1211–1223
12 Kiriazi, J., Ghali, H., Ragaie, H., Haddara, H.: 'Reconfigurable dual-band dipole antenna on silicon using series MEMS switches'. Proc. Antennas and Propagation Society Int. Symp., June 2003, pp. 403–406
13 Zheng, A.G., Chryssomallis, M., Lyke, J., Ponchak, G., Papapolymerou, J., Christodoulou, C.G.: 'Design, fabrication and measurements of an RF-MEMS-based self-similar reconfigurable antenna', *IEEE Trans. Antennas Propag., Spec. Issue Multifunction Antennas and Antenna Syst.*, 2006, **54**, (2), Part 1, pp. 422–432
14 Kingsley, N., Anagnostou, D.E., Tentzeris, M., Papapolymerou, J.: 'RF MEMS sequentially-reconfigurable sierpinski antenna on a flexible, organic substrate with novel DC bias technique', *IEEE/ASME J. Microelectromech. Syst.*, 2007, **16**, (5), pp. 1185–1192
15 Wang, G., Thompson, D., Papapolymerou, J., Tentzeris, E.M.: 'Low cost RF MEMS switch using LCP substrate'. European Microwave Conf., October 2004, pp. 1441–1444
16 Sarkar, S., Palazarri, V., Wang, G., *et al.*: 'LCP and RF MEMS SOP technology for reconfigurable and multi-band RF and mm-wave integrated module'. IEEE MTT-S Int. Microwave Symp. Digest, June 2004, pp. 567–570
17 Thompson, D.C., Tantot, O., Jallageas, H., Ponchak, G.E., Tentzeris, M.M., Papapolymerou, J.: 'Characterization of liquid crystal polymer (LCP) material and transmission lines on LCP substrates from 30-110 GH2', *IEEE Trans. Microw. Theory Tech.*, 2004, **52**, (4), pp. 1343–1352